Open Access

Recent Progress in Materials

LIDSEN Publishing Inc.

Original Research

^{7}Li Diffusion in Thin Disks of Single-Crystal Garnet LLZO-Ta Studied by PFG-NMR Spectroscopy

Kikuko Hayamizu [1,*], Tomoyuki Haishi [2], Yasuhiko Terada [1], Kunimitsu Kataoka [3], Junji Akimoto [3]

1. Tsukuba University, Tsukuba, Japan; E-Mails: hayamizu.k3@gmail.com; terada.yasuhiko.fu@u.tsukuba.ac.jp
2. MRTechnology, Tsukuba, Japan; E-Mail: tomoyuki.haishi.mrtechnology@gmail.com
3. National Institute of Advanced Industrial Science and Technology, AIST Tsukuba Centre 5, Japan; E-Mails: kataoka-kunimitsu@aist.go.jp; j.akimoto@aist.go.jp

* **Correspondence:** Kikuko Hayamizu; E-Mail: hayamizu.k3@gmail.com

Academic Editor: Eugene S. Mananga

Special Issue: Advanced Nuclear Magnetic Resonance in Batteries and Fuel Cells Research

Recent Progress in Materials
2023, volume 5, issue 2
doi:10.21926/rpm.2302014

Received: January 24, 2023
Accepted: March 26, 2023
Published: April 03, 2023

Abstract

Pulsed field-gradient (PFG) NMR spectroscopy was applied to thin disk samples (0.5, 1 and 2 mm thick, 4 mm diameter) of LLZO-Ta ($Li_6La_3Zr_{1.5}Ta_{0.5}O_{12}$) single crystal. We have measured the diffusion of ^{7}Li in thin pellets (0.5 to 3 mm thick) of NASICON-type LAGP powder and found that the Li^{+} diffuses preferentially in the thicker direction. In this study, we placed 1 mm thick, 4 mm diameter disk-shaped single crystals vertically, i.e., parallel to the PFG direction. We found that ^{7}Li ions diffuse similarly as in rod-shaped single crystals. The ^{7}Li diffusion is slow (diffusion coefficient; $\sim 2 \times 10^{-13}$ m^2s^{-1}) at $\Delta \geq 100$ milliseconds and gradually becomes faster to $\sim 1 \times 10^{-11}$ m^2s^{-1} at $\Delta \leq 10$ milliseconds at 28°C. A diffraction pattern was observed in the echo decay plots, which was not observed in well-prepared single crystal rod samples. The diffraction patterns are often observed in powder inorganic electrolytes (LLZOs, LLTO, LAGP, and $(Li_2S)_x(P_2S_5)_y$). In this study, edge effects are assumed for the diffraction pattern of the vertically placed thin disk of the single crystal. For horizontally placed disks, at long observation times ($\Delta \geq 100$ milliseconds), the diffusion coefficients of ^{7}Li agreed with those of the rod-

shaped samples. However, as Δ became shorter, contrary to the vertically placed disk, the diffusion of ^{7}Li decreased and the plots became less linear. Surprisingly, as Δ became shorter (Δ ≤ 15 milliseconds), sinusoidal patterns were observed in the real and imaginary elements of the echo attenuation plots,. The pattern is reproducible and the first example of sinusoidal real and imaginary components of the echo attenuation plot was observed, but an adequate explanation has not been obtained.

Keywords

Pulsed field-gradient NMR (PFG-NMR); single-crystal thin disk; garnet-type LLZO-Ta ($Li_6La_3Zr_{1.5}Ta_{0.5}O_{12}$); time-dependent diffusion of ^{7}Li; sinusoidal patterns in real and imaginary components

1. Introduction

The development of solid-state Li batteries is being urged to industrial needs at the present stage, and many investigations are being conducted. Since the studies are spread over a wide-range, many review papers, particularly on solid inorganic electrolytes, have been published. The studies are continuously conducted to contribute achievements of all-solid-state lithium batteries. In inorganic solid electrolytes, Li diffusion is supposed to cause ionic conductivity. Then, solid-state $^{6, 7}$Li NMR spectroscopy has been conducted long in this research field. In the present study we concern with the ^{7}Li pulsed field-gradient (PFG)-NMR spectroscopy for the ^{7}Li diffusion in thin disk samples of single-crystal garnet-type LLZO-Ta ($Li_6La_3Zr_{1.5}Ta_{0.5}O_{12}$).

NMR spectroscopy has played important roles in the studies of ion-conductive inorganic solids from an early stage of this field [1-4]. The diffusional (translational) motion of atoms was theoretically surveyed in connection to ionic conduction in 1994 [1]. The approaches to the conducting nuclei (mainly $^{6, 7}$Li) by spin-lattice relaxation times with various modes were proposed and summarized in 2005 [2] and expanded to techniques with wider time scales ($T_{1\rho}$, spin-alignment echo). Ion conducting solid-state materials have short- and long-range orders, and the research approaches by solid-state NMR techniques were reviewed in 2010 [3]. By PFG-NMR method reviewed mass transfer in mesoporous materials in 2013 [4].

We have been interested in ion diffusion in liquid electrolytes and studied the relations between ionic conductivity and anion and cation diffusion coefficients [5]. In addition, we also measured ^{7}Li diffusion in solid electrolytes and found the phenomena are quite different from those of diffusion in liquid states. We have reviewed the studies on ^{7}Li diffusion phenomena for solution electrolytes, ionic liquids, and solid inorganic electrolytes in a chapter [6]. Review articles on NMR investigation of solid electrolytes for lithium batteries [7, 8] and widespread techniques including NMR for the studies of ion transfer mechanisms in crystalline materials were published [9]. A new dynamic nuclear polarization (DNP) technique on battery materials was also reviewed [10].

Due to their high safety and high energy density, all-solid-state batteries are expected to be used in electric vehicle (EV). Great demands await their realization. In practice, however, many problems remain to be improved. As one of the attempts, the thin solid electrolytes have been proposed [11, 12] and reviewed [13].

The PFG-NMR explicitly includes time-scale and space-scale concepts. The experiments are performed by application of two pulsed field gradients (PFG). The PFG, G_z is applied along the z-direction of the external magnetic field G_0. The pulse sequences of the PFG-NMR method are shown in Figure 1 for (a) Hahn echo PFG and (b) Stimulated echo (STE) PFG methods.

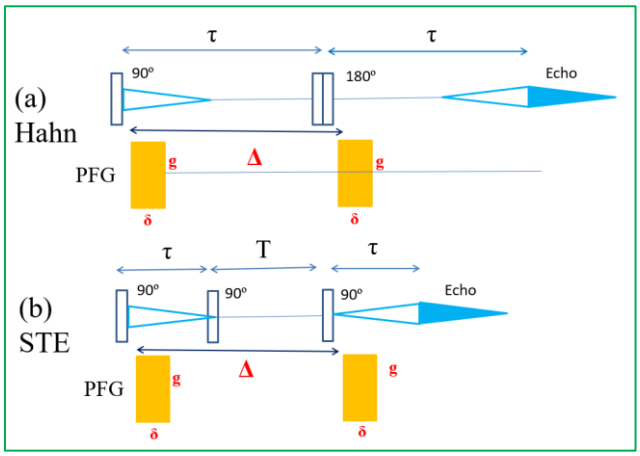

Figure 1 The pulse sequences for (a) Hahn echo PFG and (b) Stimulated echo (STE) PFG, in which two PFGs of intensity *g* and duration time δ are applied with the diffusion time Δ. When T_2 is short, the STE pulse sequence is used. Time interval τ in (a) and (b) is related T_2 and T in (b) is related to T_1.

Hahn pulse sequence (90°-τ-180°-τ-echo (acquisition)) affords T_2 by changing τ values and plotting the exponential decay of the echo signals for the T_2 process. Inserting the two PFGs of intensity *g* and duration time δ with the diffusion time Δ enables us to measure the diffusion coefficient by plotting the Stejskal and Tanner equation. The echo attenuation, *E*, is related to the diffusion coefficient, *D*, for a homogeneous system [14, 15].

$$S(g,\delta,\Delta) = \frac{E}{E_0} = \exp\left(-\gamma^2\delta^2 g^2 D\left(\Delta - \frac{\delta}{3}\right)\right) = \exp(-bD) \quad (1)$$

$$b = \gamma^2\delta^2 g^2\left(\Delta - \frac{\delta}{3}\right),$$

where γ is the ^{7}Li gyromagnetic ratio, by varying $g \times \delta$, the echo attenuation, *E*, can be measured, normalized by E_0 near $g \times \delta$ = zero, and plotted versus *b* ($\gamma^2\delta^2g^2(\Delta-\delta/3)$ [$m^{-2}s$]) (*b*-space plot). If the sine-shaped PFG is used, the Stejskal and Tanner equation is

$$S(g,\delta,\Delta) = \frac{E}{E_0} = \exp\left(-\gamma^2\delta^2 g^2 D\frac{(4\Delta-\delta)}{\pi^2}\right) = \exp(-bD) \quad (2)$$

$$b = \frac{\gamma^2 g^2\delta^2(4\Delta-\delta)}{\pi^2},$$

where the effective PFG magnitude is about 60% reduced. The magnitude of the PFG must be calibrated, and we use an ionic liquid, 1-ethyl-3-methyl-imidazolium bis (trifluoromethyl sulfonyl) amide ([EMIm] [TFSA]) as a standard compound [16, 17]. The Stejskal and Tanner equation is based on the delta function of the PFG (short gradient pulse approximation), and the sets of δ, *g*, and Δ

used approximately satisfy the Stejskal and Tanner assumption. When the PFG is a good rectangular shape, the *D* value can be observed for a fixed *g* varying δ and for a fixed δ varying *g*. We confirmed that the *D* values agree with good accuracy either δ or *g* varied using [EMIm] [TFSA]. For reference, the Stejskal and Tanner plots of ^{7}Li diffusion in a homogeneous solution are shown in Figure S1 in Additional Materials. The measurements were performed with a fixed *g* varying δ and with a fixed δ varying *g*. Both both plot yield nearly identical values of the diffusion coefficients. The ^{7}Li diffusion in inorganic electrolytes is anomalous depending on Δ and *g*, in which the Stejskal and Tanner plot with a fixed δ varying *g,* deviates from a straight line [18, 19].

In Figure 1, the first PFG marks the initial position of the diffusing species and after a time interval Δ, the second PFG detects the position of the marked species. In the rotating frame scheme, the first 90° pulse irradiation from the x-axis causes the ^{7}Li magnetization to tilt toward the y-axis, resulting in precession in the xy-plane along the z-direction. The initial PFG affects the precession velocity; the precession phase of the ^{7}Li magnetization is encoded transversely at each location. The precession velocity varies depending on the location, and the transverse magnetization phases encoded in the xy-plane. The second PFG detects phased magnetization. The one-dimensional detection of the echo attenuation signal is performed along the z-direction; the PFG-NMR measurements can selectively observe diffusion in the z-direction and exclude diffusion in other directions.

The possible range of the diffusion coefficients (*D*) obtained by the PFG-NMR is 10^{-9}∼10^{-13} m^2s^{-1} including liquids and solids. The root mean square (RMS) value ($\sqrt{2D\Delta}$) is between 10^{-5} to 10^{-7} m at Δ = 1 × 10^{-1} s. The diffusion length is micro-meter order, and very long compared to the nanoscale (10^{-9} m), which is studied by XRD, neutron-diffraction, and the correlation times obtained from NMR relaxation times. The Li-pathways proposed by XRD and neutron diffraction are a short-range distance (∼10^{-9} m) compared with the diffusion distance observed by PFG-NMR.

By Stokes-Einstein (SE) relation connects the bulk diffusion coefficient to viscosity (η) in liquids. As shown in Figure S2 in Additional Materials, we demonstrated that the relationship between *D* and η is linear over a wide temperature range in H_2O in the framework of the SE relationship [20]. The $D_{H2O} \sim 3 \times 10^{-9}$ m^2s^{-1} at ambient temperature suggests the time ranges and spatial scales of η. The diffusion in liquids is based on the concept of Brownian motion.

Nernst-Einstein (NE) relation is also important for the diffusion coefficients of cation and anion in liquids connected to ionic conductivity (σ). Since σ is defined as the number of charged ions multiplied by their velocity in unit time and unit distance, the concepts of time and spatial scale are unclear. The *D* values obtained by the PFG-NMR methods are important, because the individual values of cation (D_{Li}), anions (D_{anion}) and solvent ($D_{solvent}$) are available. For solution electrolytes the NE equation is valid [5], and the time and space scales of ionic conductivity and diffusion coefficient should be comparable.

The anions of inorganic solid electrolytes constitute the inorganic solid skeleton and are fixed without translational motion. The electric conductivity σ is carried by diffusing Li^+ only. The relation between σ and the diffusion coefficient of Li^+ at temperature T, is written by equation (3) as

$$D_{Li}(T) = \frac{kT}{N_{NE}e^2}\sigma(T) \tag{3}$$

where *k* is the Boltzmann constant and *e* is the elementary charge [21]. N_{NE} is the number of carrier

ions and can be written as

$$N_{NE} = \frac{kT\sigma(T)}{e^2 D_{Li}(T)} \quad (4)$$

When the experimental data on the temperature-dependent experimental values of the σ and D_{Li} are available, the temperature-dependent number of diffusion Li^+ (N_{NE}) can be estimated. The value of N_{NE} is related to the degree of ion dissociation in liquid electrolytes, and the mobility of Li^+ in inorganic solid electrolytes.

^{7}Li (I = 3/2) is a quadrupolar nucleus and quadrupole constant is defined as $C_q = e^2qQ/h$ (Hz unit), whose values have been reported from 20 to 120 kHz. The theoretical spectrum is a triplet of the spacing $C_q/4$ and relative intensity 3:4:3 [22]. The observed spectra were reported for single crystal $LiTaO_3$ for ^{7}Li [23] and powder $NaNO_3$ for ^{23}Na [24]. The temperature-dependent ^{7}Li spectral patterns were reported for single-crystal $LiAlO_2$ [25]. Generally, the spatial averaging of the electric field gradient is necessary for the powder samples, and the typical spectral pattern for the I = 3/2 nucleus is shown in Abragam [22]. The temperature-dependent patterns are reported for NASICON-type LATP [26], LAGP and LAGPT [27] and sulfide electrolyte $Li_{10}SnP_2S_{12}$ [28]. The sample in this study, LLZO has cubic symmetry and $C_q = 0$ without satellite peaks.

In most inorganic solid electrolytes Li sites have been reported to be non-uniform; Li^+ are located at multiple sites, disordered sites, or defects. ^{7}Li spectra are overlapped with different ^{7}Li shifts of various line widths and intensities. The sharp ^{7}Li line is supposed to have long T_2 which contributes to the echo signal, and broad lines with shorter T_2 are not observed in the echo signal. Since PFG-NMR measures the echo signal, only sharp components are observed in diffusion measurements.

We have reported diffusion of ^{7}Li in inorganic solid electrolytes for powder samples under different PFG parameters (diffusion time Δ and PFG intensity *g*) with varying temperatures of garnets $Li_7La_3Zr_2O_{12}$ (LLZO) and $Li_{6.6}La_3Zr_{1.6}Ta_{0.4}O_{12}$ (LLZO-Ta) [18, 29], NASICON-type LAGP ($Li_{1.5}Al_{0.5}Ge_{1.5}(PO_4)_3$) [30, 31], perovskite-type $Li_{0.33}La_{0.55}TiO_3$ (LLTO) [32], and sulfide-based solid electrolytes $(Li_2S)_x(P_2S_5)_y$ [33-35]. They have high ionic conductivity (≤10^{-4} S cm^{-1}), and are candidates to produce all-solid-state lithium-ion batteries.

Anomalous Li diffusion phenomena were observed; in short Δ, Li^+ diffuses fast in random manners and in longer Δ, the Li^+ diffusion gradually slows down and uniform. When Δ is short, fast-moving Li^+ and slow-moving Li^+ coexist, and faster-moving species can be detected by smaller *g* and the slower-moving species need to be detected at larger *g* [19, 29, 30]. In the solid inorganic electrolytes, the Δ and *g*-dependent diffusion of Li^+ affords the apparent diffusion coefficient ($D_{apparent}$), which is different from the diffusion of ions in continuous and homogeneous bulk media like solution electrolytes. The diffracted patterns appear for short Δ (≥15 milliseconds) with faster diffusion: the fast-moving Li^+ shows a diffracted pattern in the echo attenuation plot for short Δ. The diffracted patterns have been widely reported as "restricted diffusion" for gas or liquid in confined spaces such as pores for long Δ [36]. On the other hand, the Li pathway in solid electrolytes is not widely spread out like in liquids. Therefore, we assume that the fast-moving Li^+ are diffracted by impinging on grain boundaries/surfaces.

In this situation, single crystal samples of LLZO-Ta ($Li_{6.5}La_3Zr_{1.5}Ta_{0.5}O_{12}$) and LLZO-Nb

($Li_{6.5}La_3Zr_{1.5}Nb_{0.5}O_{12}$) were obtained [37-39]. The single crystal samples exhibit faster ionic conductivity than the corresponding powder samples. Regarding PFG-NMR measurements, the single-crystal samples have a longer T_2 and higher sensitivity due to higher density and are friendly for PFG-NMR measurements. We studied these single crystal samples by PFG-NMR technology as well as NMR spectroscopy [19, 40]. The results confirmed that ^{7}Li diffusion depends on Δ and the apparent diffusion constant ($D_{apparent}$) values are larger than those of the powder samples under the same measuring conditions. No diffraction pattern in the echo attenuation plot was observed in the well-prepared single-crystal rod-shaped samples, suggesting the sample is homogeneous and grain-free. The *g*-dependence was significantly reduced when compared to the crushed single-crystal and powder samples, indicating more homogeneous diffusion in the single-crystals. The reduced *g*-dependent diffusion and lack of diffraction are reasonable because the single crystals are more homogeneous with fewer obstructions in the long-range Li pathway.

From the perspective of using inorganic solid electrolytes in all solid lithium batteries, it is important to consider the relationship between ionic conductivity and Li^+ diffusion. As indicated in equation (3), the ^{7}Li diffusion coefficient (D_{Li}) is related to the ionic conductivity (σ) with a carrier number N_{NE} as a parameter. It should be noted that the diffusion of Li^+ depends on Δ and a unique and equilibrated value of D_{Li} is obtained with a long Δ. The relationships suggest the importance of the data on Li diffusion constants. Then using the temperature-dependent equilibrium D_{Li} values, the plots of D_{Li} and N_{NE} versus σ were shown for powder LLZO, LAGP, LLZO-Ta, and LLZO-Al-Ta [19]. The temperature-dependent plots of D_{Li} and N_{NE} versus σ were made to compare the powder and single-crystal garnet electrolytes [40]. The relations of D_{Li} and $N_{carrier}$ versus σ at room temperature were shown for inorganic solid electrolytes including recently reported values in Figure S3 in Additional Materials.

From the electrochemical approach, the solid samples' thickness affects all-solid batteries' performance [11-13]. Then, the thickness of the solid electrolytes may affect the diffusion pathways of Li^+ measured by the PFG-NMR. From the analogy of electrochemistry, we have observed the diffusion of ^{7}Li in the thin samples of power pellets of NASICON-type LAGP ($Li_{1.5}Al_{0.5}Ge_{1.5}(PO_4)_3$) [41]. The thickness of the pellets was 0.5 mm to 2 mm (~10^{-3} m) and sufficient length to the RMS (10^{-5} to 10^{-7} m) of ^{7}Li diffusion. The pellet samples were placed horizontally to the PFG direction (z-direction). In short Δ, the diffusion in the z-direction of ^{7}Li is very slow in the thin pellets, and the thinner the pellet the slower the ^{7}Li diffusion. The surface must influence the formation of Li pathways whose effects appeared in short Δ. As Δ becomes long, diffusion in various directions is possible and the z-component approaches the same value as the bulk powder sample [41]. The ^{7}Li prefers to diffuse in a wider direction. The long-range Li pathways are assumed to be influenced by surfaces in the thin samples. An important question is a distance to form the continuous diffusion of ^{7}Li in tortuous Li pathways in solid bulk samples.

In this study, expecting a clearer picture of the lithium pathway of single crystal samples, we prepared thin disks from a rod sample of single crystal LLZO-Ta. In a disk sample (1 mm thick, 4 mm diameter) placed vertically to the PFG direction, the diffusion of Li^+ was accountable by that of the rod-shaped single crystal LLZO-Ta. However, the diffusion in thin disks placed horizontally differed from the thin powder pellets of LAGP in the same arrangement. At short Δ, the echo attenuation plots consist of sinusoidal real and imaginary patterns.

2. Experimental

2.1 Sample Preparation

Four thin disk samples were prepared from a single crystal rod (diameter about 4 mm, length 14 mm) of cubic garnet LLZO-Ta ($Li_{6.5}La_3Zr_{1.5}Ta_{0.5}O_{12}$) using a low-speed diamond cutter placed in a drying chamber. The diameter of the disk-shaped samples was approximately 4 mm. The thicknesses were 0.5, 1, and 2 mm. The three single-crystal samples were placed horizontally in a Shigemi 5ϕ NMR micro-sample tube (Tokyo, Japan). The top and bottom of the horizontal samples are faced with glass. One thin disk sample of 1 mm was placed vertically. The sample tubes were placed parallel to the external magnetic field (z-direction) and to the pulsed-field gradient (PFG) direction, so that the Li diffusion was measured in the 0.5, 1, and 2-mm thick directions and 4-mm vertical direction for the 1-mm thick sample. The samples were sealed with instant adhesive ®Aron Alpha (Krazy Glue).

2.2 NMR Measurements

The ^{7}Li PFG-NMR spectra were measured using a JEOL (Tokyo, Japan) PFG probe placed in a 4.7 T wide-bore superconductive magnet and a monopolar amplifier (50 A). The PFG equipment produces no background DC and eddy current effects disappear less than 0.35 ms after the strong PFG application (14 Tm^{-1}) [30]. The measurements were performed at the ^{7}Li frequency of 78.5 MHz with a console of a Tecmag Apollo-NTNMR system (Houston, USA). The software Origin2022 was used to plot the measured data. Because of the short ^{7}Li T_2 and low sensitivity of the thin samples, a stimulated pulse sequence in Figure 2 was used for the ^{7}Li PFG-NMR measurements. The diffusion of Li ions was always measured by a fixed *g* varying δ using a good-shaped rectangular PFG. To evaluate the diffusion coefficient, the echo attenuation, *E*, was plotted by the Stejskal and Tanner equation (1).

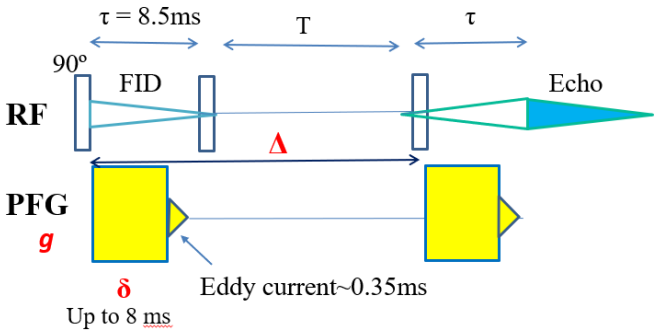

Figure 2 Stimulated PFG pulse sequence for the present measurements. The PFG is shaped to be a good rectangle for two equivalent PFGs, which enables to generate effective $g \times \delta$ with a fixed *g* and δ varied. The background DC current was not detected. The eddy current effects disappeared within 0.35 ms after the application of a PFG of 14 Tm^{-1}. In the present study, for Δ = 10 ms and longer, τ was set to 8.5 ms and δ varied with a fixed *g* (10 Tm^{-1}). The PFG interval time Δ was varied by the time interval T between the second and third 90° pulses. The PFG direction is in the z-direction along the external magnetic field B_o (parallel to a sample tube).

3. Results and Discussion

3.1 ^{7}Li Spectra

The ^{7}Li NMR spectrum of a 1-mm single-crystal LLZO-Ta placed horizontally at 28°C is shown in Figure 3(a). The ^{7}Li spectrum consists of narrow and broad components whose patterns are similar in powder LLZO-Ta [29] and LLZO [18] and as well as single crystals of LLZO-Ta [19] and LLZO-Nb [40]. It is noted that since LLZOs are spherically symmetric, the eqQ satellite peaks do not appear. From the XRD analysis of the single crystal of LLZO-Ta, Li ions occupied two interstitial sites; Li1 and Li2 ions located in distorted tetrahedral and octahedral sites, respectively [39]. The two components of ^{7}Li spectra are reasonable for the crystal structure analysis. In the present thin samples, the line widths of the broad and narrow components are slightly larger (about 2.0 and 0.18 kHz) in the horizontally placed samples than those of the vertically placed sample (about 1.6 and 0.12 kHz). The ratios of the sharp component ranged from approximately 0.52 and 0.45, respectively. The spectral center positions of the thin samples varied between -0.02 and 0 ppm from the aqueous LiCl. The echo signal was sharp without containing the broader component and the PFG-NMR measurements was performed for the narrow component.

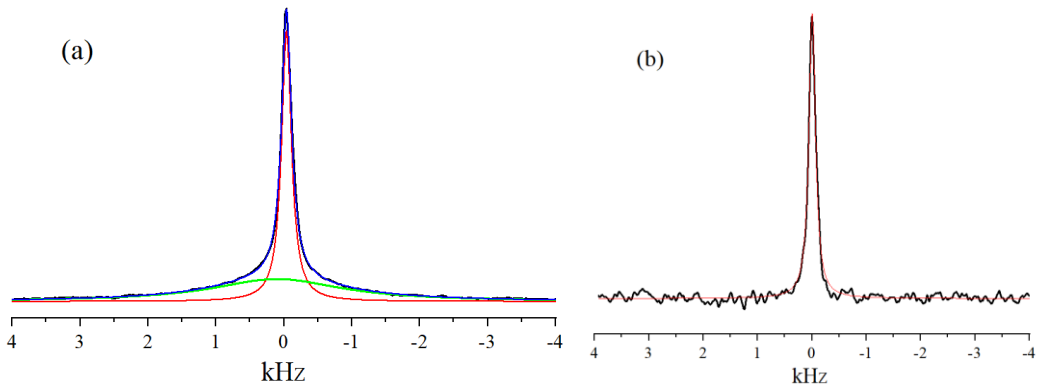

Figure 3 (a) Single-pulse ^{7}Li spectrum and (b) Hahn echo signal (τ = 10 ms) of 1 mm thick sample of single-crystal LLZO-Ta at 28°C. The line widths of the broad and narrow components were 2.2 and 0.18 kHz, respectively and the relative area ratio was almost the same. The line width of the echo signal (b) was 0.15 kHz.

3.2 ^{7}Li T_1 and T_2

To determine the PFG measuring conditions, spin-spin relaxation time, T_2 values are necessary to estimate τ value in Figure 2. The ^{7}Li T_2 values observed by the Hahn echo pulse sequence were between 5.0 and 5.8 ms at 28°C for the samples in this study. The ^{7}Li spin-lattice relaxation time, T_1 was observed by the usual inversion recovery pulse sequence and between 120 and 140 ms at 28°C, which values were consistent with previously reported block single crystals. The ^{7}Li spectrum, T_1 and T_2 values for the present thin disk samples were not sensitive to sample size.

3.3 Δ-Dependence in ^{7}Li Diffusion

We have reported the Δ-dependent Li diffusion in powder samples for four kinds of inorganic

solid electrolytes (LLZOs, LLTO, LAGP, and $(Li_2S)_x(P_2S_5)_y$). The fast ^7Li diffusion ($<10^{-11}$ m^2s^{-1}) was observed for short Δ (>15 ms), decreasing with increasing Δ value and converging to a small equilibrium value ($\sim10^{-13}$ m^2s^{-1}). For short Δ, the diffracted patterns in the echo attenuation plots were observed for these inorganic electrolytes. Previously, we reported the effects of the thickness on the ^7Li diffusion in the power pellet samples of NASICON-type LAGP ($Li_{1.5}Al_{0.5}Ge_{1.5}(PO_4)_3$) [41]. Five samples with a thickness of 0.5, 1, 2, 3 and 4 mm were measured, and the thickness dependence in diffusion was linear, i.e., thinner samples were found to have slower diffusion. At long Δ, the $D_{apparent}$ remained constant at small values for all samples ($\sim3.5 \times 10^{-13}$ m^2s^{-1}). For shorter Δ, the $D_{apparent}$ values increased with scattering. The thinner the sample, the slower the diffusion. At shorter Δ (≤10 ms) faster diffusion was observed for the thicker pellets (3 mm and 4 mm), with accompanying diffracted echo attenuation.

In our previous experiences, in the ^7Li diffusion measurements for single-crystals, the sample cutting caused significant effects, which were lifted after several days [19]. In the present study, the Li diffusion measurements were initiated two weeks after the sample preparation. The experiments were repeated approximately 2.5 years after the sample preparation, because they contained unexpected and peculiar results. This paper describes the reliable results from the initial to long-term experiments.

In the single cubic crystals LLZO-Ta and LLZO-Nb, we have reported that the Li-diffusion is observation time (Δ) dependent and the estimated diffusion coefficient became apparent diffusion coefficient ($D_{apparent}$) at a certain Δ. For shorter Δ, the $D_{apparent}$ of ^7Li is fast and in the order of 10^{-11} m^2s^{-1} at ambient temperature. When the Δ became long, the $D_{apparent}$ became slower and converged to a single value free from the observation parameters ($\sim10^{-13}$ m^2s^{-1}) at room temperature. The $D_{apparent}$ values in the single crystals are much larger than those of the corresponding powder samples at the same temperature. In the present study for the various thick samples, the D values were consistent with the almost constant values at Δ = 200 ms (Figure 4).

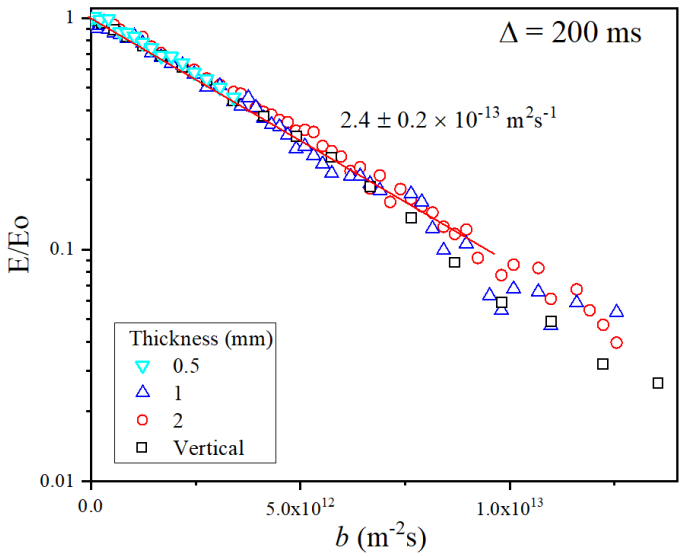

Figure 4 The Stejskal and Tanner plots at Δ = 200 ms and g = 10.0 Tm^{-1} for three thin disks (0.5, 1 and 2 mm) placed in the horizontal direction and a 1 mm thin disk placed vertically to the external magnetic field at 28°C. The diameter of the disks is about 4 mm.

In this study, we observed the Li diffusion repeatedly with g = 10 Tm^{-1} and at 28°C for the four disk samples. At Δ = 100 and 200 ms, consistent results were always obtained for the four samples and the diffusion coefficients were approximately 2.5 ± 0.2 and 2.4 ± 0.1 × 10^{-13} m^2s^{-1} for Δ = 100 and 200 ms, respectively. The values are consistent with the corresponding values of rod-shaped single-crystal LLZO-Ta [19]. Root-mean-square displacement RMS = $\sqrt{2D\Delta}$ are 0.22 and 0.31 μm for Δ = 100 and 200 ms, respectively. The values were almost consistent within the four samples and did not change after sample preparation.

As Δ became shorter, the Stejskal and Tanner plots deviated from linear plots and the pattern changed with sample thickness. The measurements were performed by varying the δ at a fixed g. For example, echo attenuation plots for the four disks are shown in Figure 5 for (a) Δ = 30 ms and (b) Δ = 10 ms. At Δ = 30 ms, the disk placed vertically showed two components and the tentative plot of the major component gave $D_{apparent}$ = 4.2 × 10^{-13} m^2s^{-1}, a little faster than the D value at Δ = 100 ms. For the 2 mm disk, a little slower $D_{apparent}$ (2.8 × 10^{-13} m^2s^{-1}) was obtained. No clear decay curves were observed for the thinner samples (1 and 0.5 mm thick), suggesting slow diffusion of ^{7}Li.

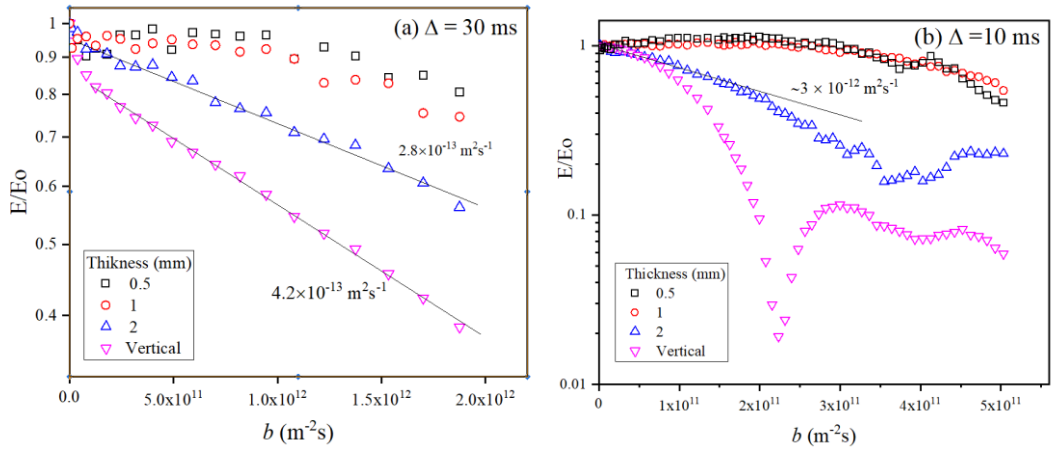

Figure 5 The Stejskal and Tanner plots at (a) Δ = 30 ms and (b) Δ = 10 ms at g = 10.0 Tm^{-1} for three thin disks (0.5, 1 and 2 mm) placed horizontally and the 1 mm disk placed vertically at 28°C.

At Δ = 10 ms (Figure 5 (b)), the echo attenuation decays for 0.5 mm and 1 mm disks were small with a little convex shape. Empirically, linear echo attenuation plots were rarely observed for very slow diffusion. The echo attenuation plot of 2 mm disk was not linear and the initial straight portion gave the $D_{apparent}$ ~3 × 10^{-12} m^2s^{-1}. The echo attenuation plot of the vertically placed disk sample showed a diffraction-like pattern. Since the well-prepared single crystal LLZO-Ta did not show a diffracted pattern even if short Δ, the diffracted pattern may be the edge effects due to the thin sample observed in the crushed and broken single crystal samples [19, 40]. For short Δ, the thickness of the disks affects different effects on the ^{7}Li diffusion.

In the present single-crystal thin disk samples, the behavior of the ^{7}Li diffusion was quite different from the powder thin pellets of LAGP [41], in which the diffusion phenomena were linear depending on the thickness of the pellets. In the present single crystal disk samples, the diffusion behaviours in the short Δ region were quite different depending on whether the 1-mm sample was placed vertically or horizontally. In order to clarify the effects, Δ-dependent ^{7}Li echo attenuation plots are shown for the 1 mm disks placed vertically in Figure 6 (a) and the comparison of Δ-dependence of

the $D_{apparent}$ values with the rod-shaped single crystal samples in Figure 6 (b), respectively.

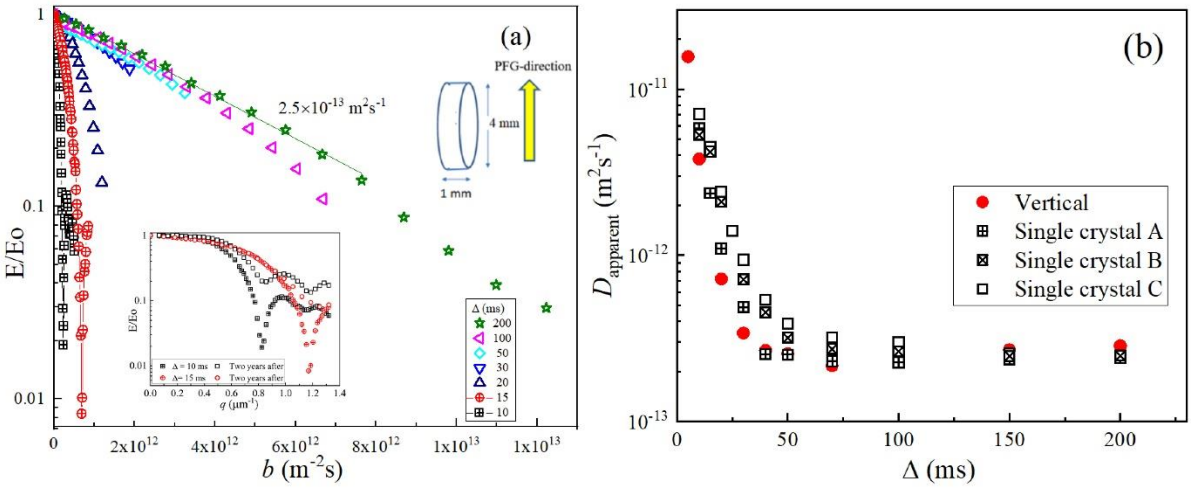

Figure 6 (a) The Δ-dependent echo-attenuation of a 1 mm disk sample placed vertically to the sample tube. The measurements were performed from Δ = 10 to 200 ms with g = 10 Tm^{-1} at 28°C. With Δ values of 10 and 15 ms, patterns with diffraction were oberved and enlarged patterns in the q-space plot are shown in the inset where the smoother paterns after two years are included. (b) The $D_{apparent}$ are plotted versus Δ for the 1 mm disk placed vertically and the reported values for the 3 rod-shaped single-crystal LLZO-Ta samples [19]. The thin disk samples showed the $D_{apparent}$ values from ~ 1.6 × 10^{-11} m^2s^{-1} (Δ = 10 ms) to 2.4 × 10^{-13} m^2s^{-1} (Δ = 200 ms).

The echo attenuation plots of the 1 mm disk placed vertically (Figure 6) resemble the plots of the well-prepared rod of LLZO-Ta and LLZO-Nb single crystals except for the diffracted patterns. The present thin disk showed the diffracted pattern at Δ = 10 and 15 ms and their expanded spectra are shown in the inset. The diffracted patterns smoothed out as the elapsed time was about two years. On the other hand, in the single rod crystal LLZO-Ta and LLZO-Nb, we have reported no diffracted patterns in the stabilized samples [19, 40]. In the thin disk, the edge effects remained in the diffracted patterns for short Δ; reasonable to the crushed powder samples of single crystals LLZO-Ta and LLZO-Nb. The $D_{apparent}$ values are plotted versus Δ for the vertically placed 1-mm disk plus reported values for different rods of single crystal LLZO-Ta and shown in Figure 6 (b). Within experimental errors, the properties are very similar to each other. The Δ-dependent diffusion behaviors in the disk (z-direction: ~ 4 mm) and rod samples are almost comparable. It can be said that the path for Li^+ to diffuse in the z-direction in a thin disk of 4 mm diameter is almost long enough.

The Δ-dependent echo attenuation plots of the 1 mm disk placed horizontally are shown in Figure 7(a), where the ^7Li diffusion was observed in the thin direction. When Δ was longer than 100 ms, the plots were linear with a gradient of ~2.5 × 10^{-13} m^2s^{-1}, consistent with the other samples (Figure 4). When Δ became shorter, the echo attenuation plots became strange, and it may be questionable that the Stejskal and Tanner equation (1) is applicable for Δ = 50 and 30 ms; the plots were a little convex. For shorter Δ, the enlarged plots are shown in Figure 7(b) between Δ = 20 and 7.5 ms, and almost no echo attenuation decay Δ = 20 and 15 ms. With the decrease of Δ, the echo attenuation curves became steeper and a tentative calculation of the echo attenuation plot at Δ = 7.5 ms was 2.9 × 10^{-12} m^2s^{-1}, and this value is a little smaller than that for the 1 mm disk placed vertically. In

contrast, the thin powder pellets of LAGP (0.5 to 2 mm) showed the ^{7}Li $D_{apparent}$ values as follows; at Δ = 20 ms the values were ~8 to 1.3 × 10^{-12} m^2s^{-1} for 0.5 to 4 mm pellets and 9 × 10^{-13} m^2s^{-1} (0.5 mm) to 4.8 × 10^{-12} m^2s^{-1} (4 mm) at Δ = 10 ms. The $D_{apparent}$ values varied smoothly with the thickness and Δ. In the LAGP powder pellet samples, the thinner the pellets, the slower the Li diffusion at shorter the Δ [41]. Contrary, the single-crystal thin disk did not show linear behavior with Δ.

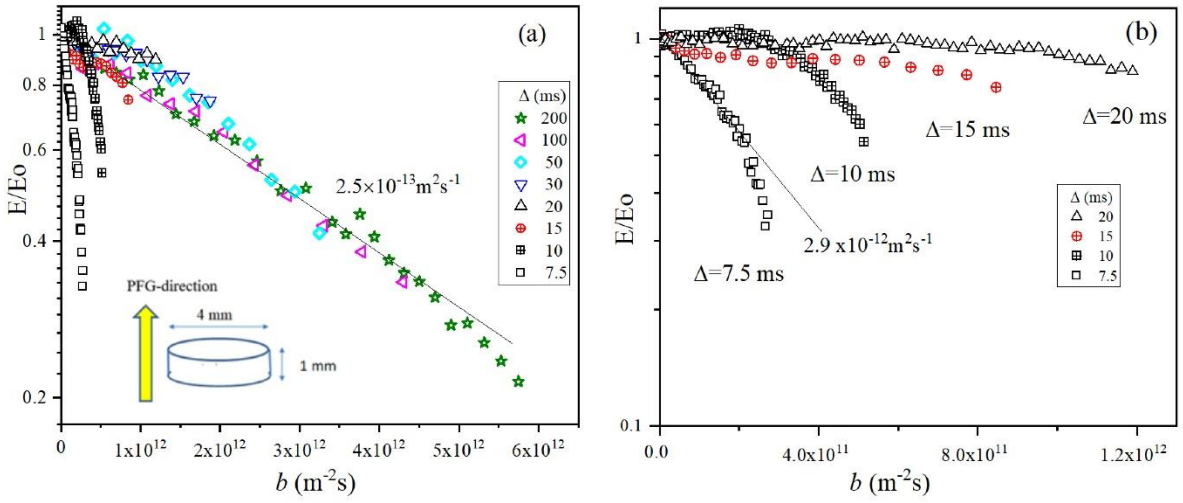

Figure 7 (a) Δ-dependent echo attenuation plots of the 1 mm disk placed horizontally in the sample tube (Δ = 7.5 to 200 ms). When Δ = 200 and 100 ms, the plots were almost linear with $D_{apparent}$ ~2.5 × 10^{-13} m^2s^{-1}. For shorter Δ values, the plots were curved. (b) Expanded echo attenuation plots for Δ = 7.5, 10, 15 and 20 ms. At Δ = 7.5 ms, $D_{apparent}$ ~ 2.9 × 10^{-12} m^2s^{-1}.

3.4 Real and Imaginary Components

In general, the free induction decay (FID) and echo precessions in the time domain are a complex function; the signal consists of real (cosine) and imaginary (sine) elements in the xy-plane, and the Fourier transformed spectrum (frequency-domain) contains phase-sensitive real and imaginary spectra. The phase adjustment is made between real and imaginary components to obtain a well-adjusted absorption spectrum. The magnitude (absolute, power) is calculated as $magnitude = \sqrt{real^2 + imaginary^2}$. Usually, the phase-sensitive absorption spectrum is adopted and the broader magnitude spectrum is rarely used. In the PFG-NMR, the echo attenuation plots are generally made of the phase-sensitive echo spectra, if each echo spectrum is properly adjusted in its phase without acquisition-related phase errors (instrumental problems). The echo attenuation plots of phase-sensitive absorption spectra of ^{7}Li can be fitted by the Stejskal and Tanner equation to give the same diffusion coefficient with the value obtained from the magnitude spectrum, if the phase adjustment is appropriate. Because the phase-sensitive absorption spectrum becomes negative at the diffracted portion, the magnitude makes the logarithm plots of E/Eo in equation (1) . For example, in Figure 8, echo profiles of magnitude, and real and imaginary elements are plotted versus δ for the diffracted pattern measured for the 1 mm disk vertically placed in Figure (4). In this measurement, Δ = 10 ms, g = 10 Tm^{-1} and δ was varied from 0.2 to 8.0 ms (60 points) and the echo attenuation is plotted versus δ. The real component showed negative values at δ was longer than 5.2 ms (Figure 6(a)), in which the diffracted pattern was observed. Note that the patterns in the q-

space are similar because of $q = (1/2\pi)\ \gamma\delta g$ [m^{-1}]. We always adopted the magnitude in the echo attenuation plots for the diffracted patterns. Actual stack plots for the magnitude and real component are shown in Figure S4 and in Figure S5 the intensities were plotted against δ and Stejskal and Tanner plot was made in Additional Materials.

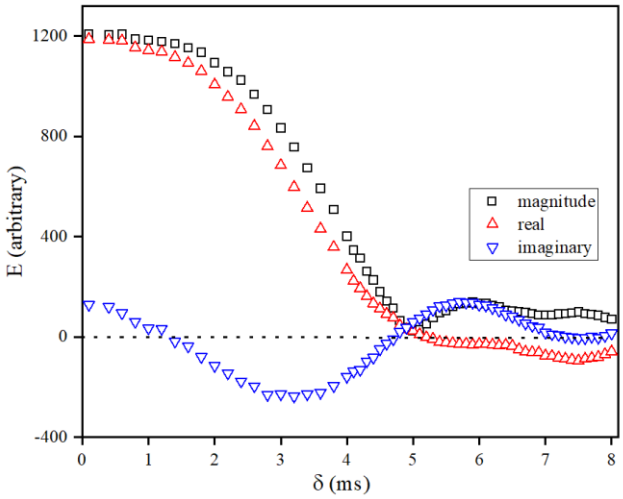

Figure 8 The echo attenuation profiles of real and imaginary components and the magnitude are shown against δ from 0.2 to 8 ms with g = 10.0 Tm^{-1} and Δ = 10 ms at 28°C. The sample is the disk (1-mm thick, 4-mm diameter) placed vertically to the PFG direction (Figure 4).

Historically, the diffraction patterns in the echo attenuation plots are known as "restricted diffusion" for diffusing gas and liquid molecules in the restricted space (~10^{-3} m) [36], where molecules diffuse fast (10^{-9}~10^{-10} m^2s^{-1}). Usually, semi-logarithmic plots of magnitude are made versus q in the diffracted decays. It is known that the inverse of q value at the diffracted point is related to the size of the restricted space.

On the other hand, in long-range Li pathways of inorganic solid electrolytes, the target space of PFG-NMR is not homogeneous and the existences of corners or grain boundaries are expected. The fast-moving Li^+ collided with such obstacles and refracted. Such collisions occur repeatedly for long intervals, and eventually the $D_{apparent}$ becomes shown down as a long Δ. For short time periods, Li^+ can diffuse fast and diffracted phenomena can be observed. At first glance, the diffracted patterns in inorganic electrolytes present the aspect of diffusion of liquid molecules in a restricted space. A different point is Δ; the diffraction is observed for long Δ in the restricted diffusion of liquid, while the Li diffusion in the solid materials the diffraction is observed in short Δ. The long-range Li pathways in μm order cannot be visualized in solid electrolytes for theoretical calculations of the echo attenuation decays. The diffracted patterns appear in magnitude and the real component may decay to minus with δ (Figure 8).

Surprisingly, we observed unbelievable phenomena for the thin disk single-crystal samples horizontally placed to the PFG. As shown in Figure 7, when Δ is shorter than 50 ms, little decay was observed in echo attenuation plots and at further shorter Δ, the decay increased again. The phenomena are different for the thin powder pellets of LAGP observed previously, in which the Li diffusion slowed linearly as the pellets thinner thinner in short Δ [41].

More surprising, for the thin single crystal disks, although the magnitude of the echo attenuation decay was small at short Δ, the real and imaginary patterns showed sinusoidal-like patterns; i.e., a "cosine curve" in the real part and a "phase-shifted sine curve" in the imaginary part as shown in Figure 9, indicating a very unusual echo attenuation behavior. Such patterns had not been seen in previous plots of echo attenuation decay, so initially we were not convinced. A stacked plots of the magnitude and phase-sensitive absorption spectra are shown in Figure S6 in Additional Materials.

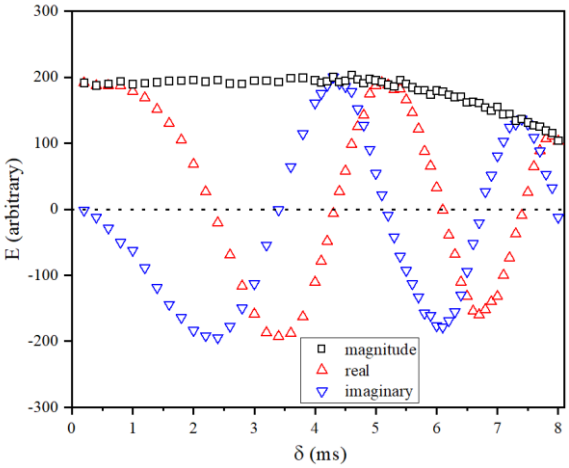

Figure 9 The echo attenuation profiles versus δ for the real and imaginary components and the magnitude are shown for the disk sample (1 mm thick, 4-mm diameter) placed horizontally to the PFG (see Figure 7(b)). The g = 10 Tm^{-1} and Δ = 10 ms at 28°C.

Figure 9 showed sinusoidal patterns of real and imaginary components, although the magnitude was slightly attenuated. At present, we cannot find out proper interpretations, but we repeated the measurements about 2.5 years, suspecting that it might be an artefact. In this paper, we describe the reliable experimental results for ^{7}Li diffusion mode when the PFG is applied to the thin direction of the disk samples.

While a sine curve is generally defined as a function of time and distance, the echo attenuation decay is defined as a function of $b = \gamma^2\delta^2g^2(\Delta-\delta/3)$ [$m^{-2}s$]) or $q = (1/2\pi)\gamma\delta g$ [m^{-1}]. Tentatively, the sinusoidal real and imaginary patterns in the q-space are simulated as cos (7.66 × q) and sin (7.66 × q + π), respectively as shown in Figure 10.

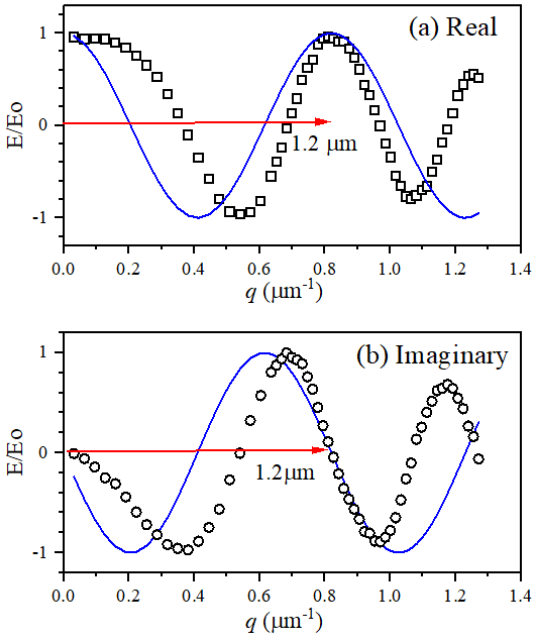

Figure 10 The tentative simulation for real and imaginary plots by cos (7.66 × *q*) and sin (7.66 × *q* + π), respectively to fit one cycle.

We cannot say the fitting by the simple cosine function is fine, since we are not convinced ourselves that this analogy is reasonable. Using the same measuring conditions, we observed the echo attenuation decay for the three disk samples placed horizontally (thickness: 0.5, 1 and 2 mm) and one disk (1 mm thickness) vertically and the real components plotted versus *q* are shown in Figure 11.

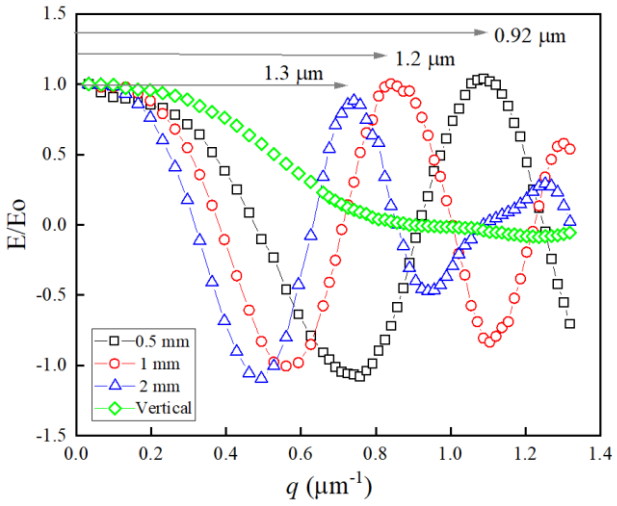

Figure 11 The real element is plotted versus *q* measured with *g* = 10 Tm^{-1}(fixed), Δ = 10 ms, and δ varied 0.2 to 8 ms at 28°C for the four thin disk samples of 0.5, 1, and 2 mm thick placed horizontally, and one disk (thickness:1 mm) placed vertically.

The three horizontally placed disk samples showed sinusoidal patterns and tentative one-cycle wavelengths were 0.92, 1.2, and 1.3 μm for 0.5-, 1-, and 2-mm samples, respectively. We used the

inverse values in q [m^{-1}] space. Clearly a wavelength was related to the thickness of diffusion direction and the smallest for the 0.5-mm sample. In short Δ, the sine-shape in real component must be related to the Li diffusion pathlength between the both side surfaces. It is not certain that standing wave concept is related. The vertical placed disk sample showed no sinusoidal pattern. The thickness is related to the sinusoidal pattern.

Next, we tried to observe the sinusoidal patterns with different Δ values for the 1-mm disk samples placed horizontally. In Figure 12, the plots of the real component are shown with Δ = 7, 10, 15 and 20 ms.

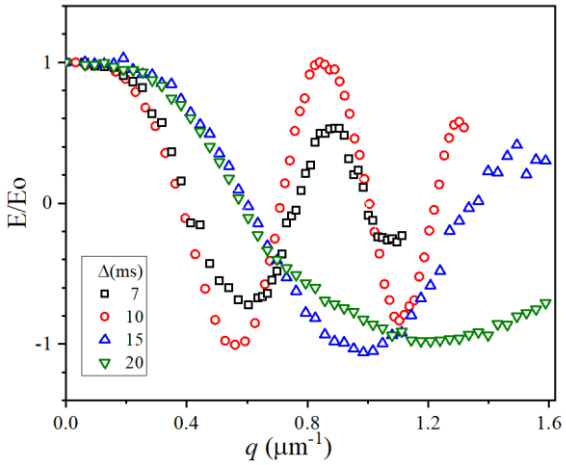

Figure 12 The q-space plot of real components of the 1-mm disk sample placed horizontally. The measurement conditions: g = 10 Tm^{-1} (fixed), δ values were varied up to 6 ms (Δ = 7 ms), 8 ms (Δ = 10 ms), and 10 ms (Δ = 15 and 20 ms) at 28°C.

The wavelength was almost the same (~1.2 μm) for Δ = 7 and 10 ms, and the sinusoidal patters become smoother as Δ increased; no clear sinusoidal patter was observed at Δ = 20 ms.

In the previous paper, we focus on the existence of structural relaxations in the single crystals and the smoothing of the surfaces after sample cutting. Good quality single crystal samples do not show diffractions after stabilization, but soon after cutting they have irregular diffraction patterns [19, 40]. For long Δ (≥100 ms), diffusion of Li^+ was insensitive to the structural relaxation including for the 0.5-mm sample. This suggested the long-range ^{7}Li diffusion is not affected by length in the z-direction.

To conform the structural relaxation, we observed repeatedly the solenoidal patterns for the 1-mm sample placed horizontally, after 2 weeks, 1 month and 1.5 years as shown in Figure 13. The one wavelength was approximately 1.2, 0.9, and 0.8 μm, respectively. The sinusoidal real pattern became smoother, and retained the pattern long times.

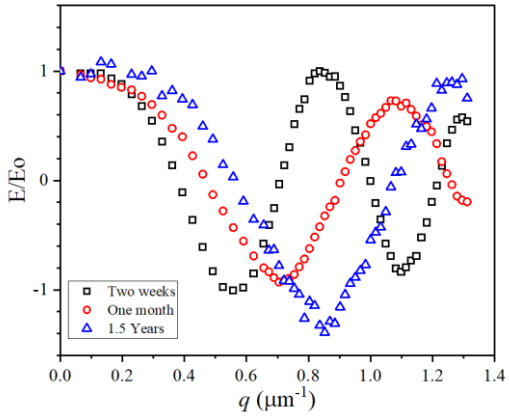

Figure 13 Structural relaxation process of the sinusoidal pattern observed by PFG-NMR for the 1-mm sample placed horizontally; 2 weeks (square), 1 month (circle) and 1.5 years (diamond) after sample preparation. Measuring conditions; g = 10.0 Tm^{-1}. Δ = 10 ms, δ varied 0.1 to 8.0 ms, stimulated pulse sequence (τ = 10 ms).

To summarize the sinusoidal patterns, (1) for the 1 mm disk, real sinusoidal patterns were observed from Δ = 7 ms to 15 ms. The shorter the Δ, the smaller the wavelength. (2) The sinusoidal patterns were observed in 0.5 to 2 mm thick disk samples. The thinner the disks, the shorter the wavelength. (3) The sinusoidal pattern was smoothed without disappearing over the time length after sample preparation. It is noted that one wavelength appearing in the real component is 0.8~1.3 μm at Δ = 10~20 ms, while the root-mean-square displacement RMS = $\sqrt{2D\Delta}$ is 0.22 and 0.31 μm for Δ = 100 and 200 ms, respectively, which is shorter than the one wavelength. It is not clear the relationship between the RMS at long Δ and the wavelength of the sinusoidal pattern in the real component at short Δ.

4. Conclusive Remarks

Diffusion of ^{7}Li was measured for thin disk samples (0.5-2 mm thick, 4 mm diameter) of a garnet-LLZO-Ta single crystal. For a thin disk sample (1 mm thick) placed vertically to the sample tube, the diffusion behavior was similar to that of a single rod crystal, with Δ-dependent $D_{apparent}$ values in close agreement. The thin disk showed diffraction patterns at short Δ, probably due to edge effects, which are different from that of the rod specimen without a diffraction pattern. This suggests that the path for Li^{+} to diffuse in the PFG direction in a thin disk sample of 4 mm diameter is almost similar to that of the rod-shaped sample.

On the other hand, thin disk samples placed horizontally showed a different behavior: Δ-dependent ^{7}Li diffusion was observed and the $D_{apparent}$ values agreed with those in the rod sample at long Δ (≥100 ms); as Δ shortened at 50 ms and 30 ms, the diffusion slowed down and almost no diffusion was observed. As Δ is further shortened, the echo attenuation plot indicates the exitance of apparent diffusion. At short Δ (≤15 ms), it is curious that the real and imaginary parts show a sinusoidal pattern, but the reason for this phenomenon is unclear. Similar echo attenuation plots have not been reported in PFG-NMR measurements. The ^{7}Li diffusion is reflected at the surface boundaries in thin single-crystal samples, possibly relating to standing wave effects. One-dimensional diffusion is observed by applying one-dimensional PFG in the same direction. The large differences in the disks between the vertical and horizontal applications suggest the length of the

lithium pathway that feels the surface effects of the single-crystal disk samples.

Acknowledgments

The authors are deeply grateful to Buichiro Ena for reading the manuscript and providing valuable comments.

Author Contributions

KH; NMR measurements and paper writing, TH; Discussed and interpretation of data, YT; Discussion, KK and JA; Preparation of the disk samples of LLZO-Ta single crystal.

Competing Interests

The authors have declared that no competing interests exist.

Additional Materials

The following additional materials are uploaded at the page of this paper.

1. Figure S1: Stejskal-Tanner plots for the Li^+ diffusion in viscous polyethylene glycol dimethyl ether (liquid) at 120 ℃ measured by Hahn echo pulse sequence. (a) *g* was fixed at 14.9 Tm^{-1} and δ varied 0.2 to 4 m for Δ= 20 and 50 ms, and δ was varied 0.2 to 3 ms. (b) δ was fixed at 2 ms and g was varied 1.04 to 14.9 Tm-1 for Δ= 20, 50, and 70 ms.
2. Figure S2: According to Stokes-Einstein relation, the diffusion coefficient D_{H2O} is plotted vs $kT/\pi\eta$ in the temperature range from -34 to 50°C.
3. Figure S3: (a) D_{Li} versus σ at room temperature except for the garnets for which the temperatures are shown; *c*-LLZO at 58°C [2], LLTO [3], LAGP [4], amorphous and crystal Li_3PS_4 [5], *β*-Li_3PS_4 [6], $Li_7S_{11}P_3$ [7, 8], LGPS [9, 10], LLZO-Ta and LLZO-Al-Ta at elevated temperatures [11] and LLZO-Ta single-crystal [12]. (b) The carrier number, $N_{carrier}$ estimated by the NE equation plotted versus σ.
4. Figure S4: Stack plots of echo attenuation spectra for the disk sample (1 mm thick, 4 mm diameter) placed vertically to the PFG direction (g = 10.0 Tm^{-1}), at Δ = 10 ms with varying δ = 0.2 to 8 ms (60 points) at 28°C.
5. Figure S5: The normalized intensities of real component and the magnitude are plotted versus δ (left) and the Stejskal and Tanner plots vs *b* in the *semi-logarithmic* graph (right).
6. Figure S6: The stack plot profiles of echo attenuation decays for a 1 mm disk sample placed horizontally to the PFG (g = 10.0 Tm^{-1}), at Δ = 10 ms with varying δ = 0.2 to 8 ms (60 pints) at 28°C.

References

1. Chadwick AV. Ionic conduction and diffusion in solids. Digit Encycl Appl Phys. 1994. doi: 10.1002/3527600434.eap187.
2. Heitjans P, Schirmer A, Indris S. NMR and β-NMR studies of diffusion in interface-dominated and disordered solids. In: Diffusion in condensed matter. Berlin, Heidelberg: Springer; 2005. pp. 367-415.

3. Eckert H. Short and medium range order in ion-conducting glasses studied by modern solid state NMR techniques. Z Phys Chem. 2010; 224: 1591-1654.
4. Kärger J, Valiullin R. Mass transfer in mesoporous materials: The benefit of microscopic diffusion measurement. Chem Soc Rev. 2013; 42: 4172-4197.
5. Hayamizu K. Direct relations between ion diffusion constants and ionic conductivity for lithium electrolyte solutions. Electrochim Acta. 2017; 254: 101-111.
6. Hayamizu K. ^{7}Li spin echo NMR diffusion studies. Annu Rep NMR Spectrosc. 2019; 98: 57-123.
7. Morales DJ, Greenbaum S. NMR investigations of crystalline and glassy solid electrolytes for lithium batteries: A brief review. Int J Mol Sci. 2020; 21: 3402.
8. Han KS, Bazak JD, Chen Y, Graham TR, Washton NM, Hu JZ, et al. Pulsed field gradient nuclear magnetic resonance and diffusion analysis in battery research. Chem Mater. 2021; 33: 8562-8590.
9. Gao Y, Nolan AM, Du P, Wu Y, Yang C, Chen Q, et al. Classical and emerging characterization techniques for investigation of ion transport mechanisms in crystalline fast ionic conductors. Chem Rev. 2020; 120: 5954-6008.
10. Haber S, Leskes M. Dynamic nuclear polarization in battery materials. Solid State Nucl Magn Reson. 2022; 117: 101763.
11. Kotobuki M, Lei H, Chen Y, Song S, Xu C, Hu N, et al. Preparation of thin solid electrolyte by hot-pressing and diamond wire slicing. RSC Adv. 2019; 9: 11670-11675.
12. Mousavi T, Chen X, Doerrer C, Jagger B, Speller SC, Grovenor CR. Fabrication of $Li_{1+x}Al_xGe_{2-x}(PO_4)_3$ thin films by sputtering for solid electrolytes. Solid State Ion. 2020; 354: 115397.
13. Wu J, Yuan L, Zhang W, Li Z, Xie X, Huang Y. Reducing the thickness of solid-state electrolyte membranes for high-energy lithium batteries. Energy Environ Sci. 2021; 14: 12-36.
14. Stejskal EO, Tanner JE. Spin diffusion measurements: Spin echoes in the presence of a time-dependent field gradient. J Chem Phys. 1965; 42: 288.
15. Tanner JE. Use of the stimulated echo in NMR diffusion studies. J Chem Phys. 1970; 52: 2523.
16. Hayamizu K, Tsuzuki S, Seki S, Umebayashi Y. Nuclear magnetic resonance studies on the rotational and translational motions of ionic liquids composed of 1-ethyl-3-methylimidazolium cation and bis (trifluoromethanesulfonyl) amide and bis (fluorosulfonyl) amide anions and their binary systems including lithium salts. J Chem Phys. 2011; 135: 084505.
17. Hayamizu K. On accurate measurements of diffusion coefficients by PGSE NMR methods (Version 2). Room-temperature ionic liquids [Internet]. 2015 [cited date 2023 December 10]. Available from: https://diffusion-nmr.jp/.
18. Hayamizu K, Seki S, Haishi T. Lithium ion micrometer diffusion in a garnet-type cubic $Li_7La_3Zr_2O_{12}$ (LLZO) studied using ^{7}Li NMR spectroscopy. J Chem Phys. 2017; 146: 024701.
19. Hayamizu K, Terada Y, Kataoka K, Akimoto J. Toward understanding the anomalous Li diffusion in inorganic solid electrolytes by studying a single-crystal garnet of LLZO–Ta by pulsed-gradient spin-echo nuclear magnetic resonance spectroscopy. J Chem Phys. 2019; 150: 194502.
20. Hayamizu K, Chiba Y, Haishi T. Dynamic ionic radius of alkali metal ions in aqueous solution: A pulsed-field gradient NMR study. RSC Adv. 2021; 11: 20252-20257.
21. Julien C, Nazri GA. Solid state batteries: Material design and optimization. Boston: Kluwer Academic Publishers; 1994.
22. Abragam A. The principles of nuclear magnetism. Oxford: Oxford university press; 1961.
23. Man PP. Measurement quadrupolar coupling with a two-pulse sequence in solid-state NMR.

Mol Phys. 1990; 69: 337-346.
24. Man PP. Study of a spin 3/2 system by a spin-echo sequence. Mol Phys. 1991; 72: 321-331.
25. Indris S, Heitjans P, Uecker R, Roling B. Li ion dynamics in a $LiAlO_2$ single crystal studied by ^7Li NMR spectroscopy and conductivity measurements. J Phys Chem C. 2012; 116: 14243-14247.
26. Emery J, Šalkus T, Barré M. NMR investigations in $Li_{1.3}Al_{0.3}Ti_{1.7}(PO_4)_3$ ceramics part II: Lithium dynamics, experiments, and model. J Phys Chem C. 2016; 120: 26235-26243.
27. Vyalikh A, Schikora M, Seipel KP, Weigler M, Zschornak M, Meutzner F, et al. NMR studies of Li mobility in NASICON-type glass-ceramic ionic conductors with optimized microstructure. J Mater Chem A. 2019; 7: 13968-13977.
28. Kaus M, Stöffler H, Yavuz M, Zinkevich T, Knapp M, Ehrenberg H, et al. Local structures and Li ion dynamics in a $Li_{10}SnP_2S_{12}$-based composite observed by multinuclear solid-state NMR spectroscopy. J Phys Chem C. 2017; 121: 23370-23376.
29. Hayamizu K, Matsuda Y, Matsui M, Imanishi N. Lithium ion diffusion measurements on a garnet-type solid conductor $Li_{6.6}La_3Zr_{1.6}Ta_{0.4}O_{12}$ by using a pulsed-gradient spin-echo NMR method. Solid State Nucl Magn Reson. 2015; 70: 21-27.
30. Hayamizu K, Seki S. Long-range Li ion diffusion in NASICON-type $Li_{1.5}Al_{0.5}Ge_{1.5}(PO_4)_3$ (LAGP) studied by ^7Li pulsed-gradient spin-echo NMR. Phys Chem Chem Phys. 2017; 19: 23483-23491.
31. Hayamizu K, Seki S, Haishi T. Non-uniform lithium-ion migration on micrometre scale for garnet- and NASICON-type solid electrolytes studied by ^7Li PGSE-NMR diffusion spectroscopy. Phys Chem Chem Phys. 2018; 20: 17615-17623.
32. Hayamizu K, Seki S, Haishi T. ^7Li NMR diffusion studies in micrometre-space for perovskite-type $Li_{0.33}La_{0.55}TiO_3$ (LLTO) influenced by grain boundaries. Solid State Ion. 2018; 326: 37-47.
33. Hayamizu K, Aihara Y. Lithium ion diffusion in solid electrolyte $(Li_2S)_7(P_2S_5)_3$ measured by pulsed-gradient spin-echo ^7Li NMR spectroscopy. Solid State Ion. 2013; 238: 7-14.
34. Hayamizu K, Aihara Y, Machida N. Anomalous lithium ion migration in the solid electrolyte $(Li_2S)_7(P_2S_5)_3$; fast ion transfer at short time intervals studied by PGSE NMR spectroscopy. Solid State Ion. 2014; 259: 59-64.
35. Hayamizu K, Aihara Y, Watanabe T, Yamada T, Ito S, Machida N. NMR studies on lithium ion migration in sulfide-based conductors, amorphous and crystalline Li_3PS_4. Solid State Ion. 2016; 285: 51-58.
36. Callaghan PT. Translational dynamics & magnetic resonance. Oxford: Oxford University Press; 2011.
37. Kataoka K, Nagata H, Akimoto J. Lithium-ion conducting oxide single crystal as solid electrolyte for advanced lithium battery application. Sci Rep. 2018; 8: 9965.
38. Kataoka K, Akimoto J. Lithium-ion conductivity and crystal structure of garnet-type solid electrolyte $Li_{7-x}La_3Zr_{2-x}Ta_xO_{12}$ using single-crystal. J Ceram Soc Jpn. 2019; 127: 521-526.
39. Kataoka K. Oxide single crystals with high lithium-ion conductivity as solid electrolytes for all-solid-state lithium secondary battery applications. J Ceram Soc Jpn. 2020; 128: 7-18.
40. Hayamizu K, Terada Y, Kataoka K, Akimoto J, Haishi T. Relationship between Li^+ diffusion and ion conduction for single-crystal and powder garnet-type electrolytes studied by ^7Li PGSE NMR spectroscopy. Phys Chem Chem Phys. 2019; 21: 23589-23597.
41. Hayamizu K, Haishi T. Ceramic-glass pellet thickness and Li diffusion in NASICON-type LAGP ($Li_{1.5}Al_{0.5}Ge_{1.5}(PO_4)_3$) studied by pulsed field gradient NMR spectroscopy. Solid State Ion. 2022; 380: 115924.